



Special Issue – 8<sup>th</sup> International Conference on Mechanical and Industrial Engineering, October 24 – 25, 2024 at The Nelson Mandela African Institute of Science and Technology, Arusha - Tanzania

## Wet gas metering performance using conventional flow measurement devices

Vitalis Mwinyi\*

Legal and Industrial Metrology, College of Business Education, P. O. Box 1968, Dar es Salaam, Tanzania.

\*Corresponding Author's E-mail: [vitalis.mwinyi@cbe.ac.tz](mailto:vitalis.mwinyi@cbe.ac.tz);

### ABSTRACT

The demand for and production of natural wet gas from wells has significantly risen in recent years. Although natural gas liquids hold substantial value in the oil and gas market, their presence in wet gas adversely affects gas metering, leading to overreading during measurement. A comprehensive study has been undertaken to formulate and enhance correlations for rectifying overreading in wet gas metering. Nevertheless, most current correlations are designed for horizontal configurations of traditional meters. Mitigating this constraint is crucial to consider the impact of gravity on pressure loss in vertically oriented systems. This study seeks to evaluate the efficacy of wet gas overreading correlations utilizing a vertically positioned Venturi flow meter, a recognized instrument for single-phase flow measurement. This project innovatively examines the influence of liquid film formation and flow along the walls of the pressure measurement zone within the Venturi tube. This liquid coating influences differential pressure, and its influence on wet gas overreading correction will be examined using established correlations.

### ARTICLE INFO

Submitted: **Apr. 23, 2024**

Revised: **Nov. 26, 2024**

Accepted: **April, 30, 2025**

Published: **June, 2025**

**Keywords:** Two-phase flow, Annular flow measurements, Natural gas measurements, Venturi measurements, Wet gas flow metering.

### INTRODUCTION

Wet gas flow (WGF) refers to a gas flow which includes a minor quantity of liquid (Salehi et al., 2024). Steven (2002) estimates gas volume by characterizing wet gas as a specific two-phase flow with a gas volume percentage above ninety-five. Wet-gas flow is characterized as the movement of gas and liquids with a Lockhart-Martinelli parameter (LMP),  $X$ , within the range  $0 < X \leq 0.3$  (Chinello et al., 2019; Graham et al., 2020). The Martinelli parameter quantifies the 'wetness' of WGF. In the oil and gas sector, moist gas flow is differentiated from multiphase flow despite both being categories of two-phase flow

(Figure 1). Hall and Steven (2007) characterize multiphase flow as the movement of gas and liquid containing multiple liquid components (hydrocarbon and water), with the gas volume fraction (GVF) ranging from 0% to 100% (ISO/TR 12748, 2015). When the multiphase flow meets the criteria ( $GVF \geq 95\%$  or  $0 < X \leq 0.3$ , where  $X$  is an LMP), the flow is classified as a multiphase WGF. WGF metering, a relatively new field, has been studied for over 30 years (Chinello, 2019). It uses a single-phase flow metering methodology to accurately quantify gas in the presence of liquid constituents like condensate and water. This study uses the

Venturi tube, a differential pressure meter, following ISO5167-04 principles (ISO5167-04, 2003) (Graham et al., 2015).

Natural gas, a fossil fuel principally consisting of methane, is extracted from “natural gas” or “crude oil wells” as wet natural gas (EIA, 2020). This gas contains natural gas liquids (NGLs) and non-hydrocarbon gases like sulfur, helium, nitrogen, hydrogen sulfide, carbon dioxide,

and water vapour. On the other hand, dry gas is processed to remove NGLs and water vapour, leaving primarily methane. The LM parameter range indicates that higher NGL content and greater gas “wetness” can occur when the LM parameter exceeds 0.3. This research chiefly aimed to enhance vertical alignment with wet gas venturi metering, which has hardly been studied.

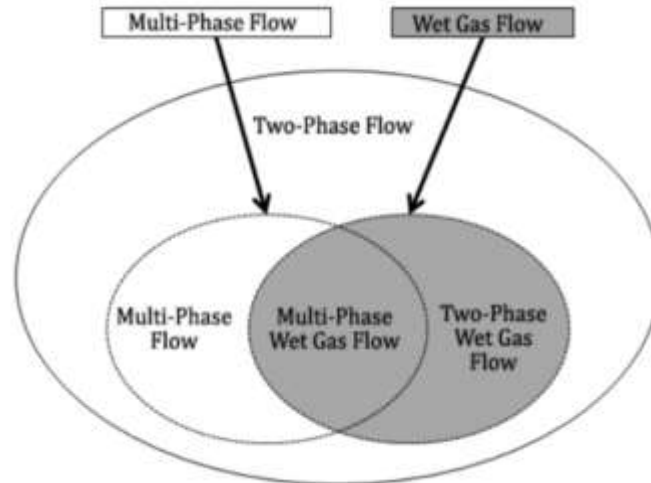
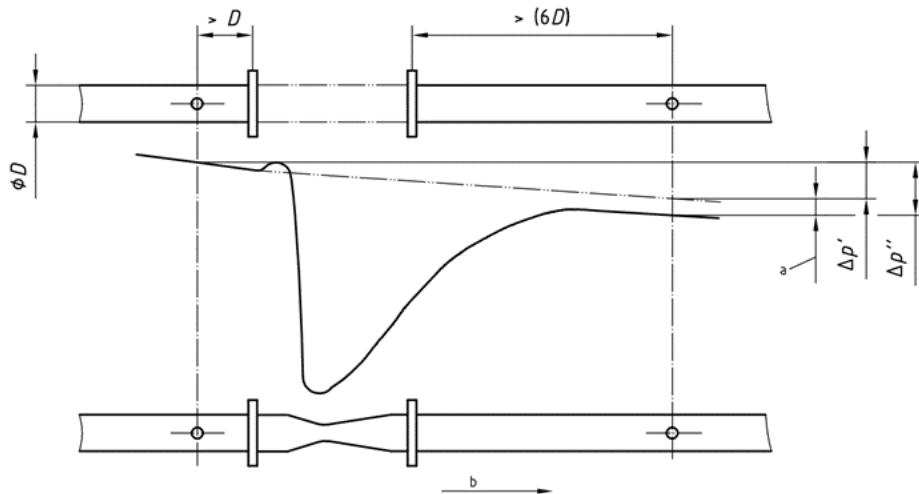


**Figure 1. The subset of a two-phase flow showing multiphase and WGF (ISO/TR 12748, 2015)**

### Pressure Drop in Conventional Flow Measuring Devices

The measurement of flow rate via traditional devices (D.P. flow meters) is mostly contingent upon the pressure differential across the specified zones (Li et al., 2020). Conventional meters include cone meters, flow nozzles, venturi tubes, orifice plates, and similar devices (Liu et al., 2020). Figure 2 illustrate the orientation of the installed, differential pressure meter, which in turn it influences the pressure drop across the constriction. Figure 2 shows the effect of frictional forces (static, dynamic,

and interfacial) and hydrostatic effects resulting from gravitational force (Liu et al., 2020). The demand for differential pressure meters in FM is due to their benefits over other varieties. The advantages encompass their typical affordability, reliance on a comprehensible principle, sturdy and straightforward construction, and applicability for metering diverse fluids and gases in single-phase flow (Flowmeters, 2015). Additionally, they have been extensively utilized and studied in flow of the wet gas (Zheng et al., 2016).



Note: “a” is the pressure loss, and “b” is the flow direction

Source: ISO5167-04 (2003)

**Figure 2: Dropping of pressure through a Venturi tube**

**Mass flow rate in differential pressure flow meters**

The differential pressure devices work under the operational principles which is known as analogous (Liu et al., 2020). It is based on the laws of energy and mass conservation, specifically, Bernoulli’s equations as shown by equations (1) and (2) and the continuity equation as shown by equation (3). Differential pressure devices function by partially impeding pipe flow to generate pressure differentials upstream and downstream, as established by energy and mass conservation principles, Bernoulli’s equations, and continuity equations (Liu et al., 2020).

$$P + \frac{1}{2}\rho v^2 + \rho g z = \text{constant} \tag{1}$$

$$P_1 + \frac{1}{2}\rho_1 v_1^2 + \rho_1 g z_1 = P_2 + \frac{1}{2}\rho_2 v_2^2 + \rho_2 g z_2 \tag{2}$$

$$\rho_1 A_1 V_1 = \rho_2 A_2 V_2 = Q_m \tag{3}$$

The main condition for equation (1) is that the flow is presumed to be incompressible and it is within a single phase. Thus,  $\rho_1 = \rho_2$ . Hence

$$A_1 V_1 = A_2 V_2 \tag{4}$$

So, when making assumptions:  $A_2 < A_1$  then  $v_2 > v_1$ , this results to  $p_2 > p_1$

Consequently, when the cross-sectional area diminishes among two places, the flow velocity escalates, and conversely, when the velocity diminishes between two sites, the pressure amplifies. If horizontal flow is assumed to be in the differential pressure meter, the values  $z_1 = z_2$  (equation (2)) shows that, by combining equations (2) and (4),  $\Delta p$ , can be correlated to the fluid velocity change (for little height variation and incompressible flows) (Collins & Clark, 2013)

$$p_1 - p_2 = \frac{1}{2}\rho(v - v_1^2) \tag{5}$$

$$\Delta p = \frac{1}{2}\rho(v_2^2 - v_1^2) \tag{6}$$

$$\Delta p = \frac{\rho v_1}{2} \left( \left( \frac{A_1}{A_2} \right)^2 - 1 \right) \tag{7}$$

Therefore, Equation 7 can result to equation (8) when rearranging it. The mass fluid flow rate ( $Q_m$ ) is shown by equation (8):

$$Q_m = \frac{A_1}{\sqrt{\left( \frac{A_1}{A_2} \right)^2 - 1}} \sqrt{2\rho\Delta p} \tag{8}$$

Equation (8) can be refined, allowing the gas mass flow rate to be articulated as follows:

$$Q_{mg} = \frac{A_2}{\sqrt{1-\beta^4}} \sqrt{2\rho_{1,g}\Delta p_g} \quad (9)$$

$$\text{Beta Ratio, } \beta = \frac{d}{D} \quad (10)$$

Whereby: d = the throat diameter D = pipe diameter at the inlet

Two coefficients are incorporated into the Equation. (9) to enhance its accuracy. The discharge coefficient, Cd, accounts for viscous influence, while the expansibility term ( $\epsilon$ ) compensates for the fluid density difference leading from the increase of velocity among the pipe and throat diameters (Collins & Clark, 2013). Therefore, the fundamental equation outlined in the standard specification (ISO5167-04, 2003) establishes a relationship between the differential pressure across the Venturi and the mass flow rate, as presented in Equation (11).  $\rho_{1g}$  is the gas density.

$$Q_{mg} = \frac{C_d \epsilon}{\sqrt{1-\beta^4}} \frac{\pi d^2}{4} \sqrt{2\rho_{1,g}\Delta p_g} \quad (11)$$

## Wet Gas Metering (WGM) Using Venturi Meter

### Venturi tube WGM for horizontal flow

The Venturi tube is a popular flow meter for wet gas measurement, particularly when adjusting for liquid content flow (ASME, 2008; Zheng et al., 2016). The meter's differential pressure reading exceeds the measured value if only the gas phase flows. The anticipated mass flow rate ( $Q_{mgs}$ ), considers mixed fluid properties.

$$Q_{mgs} = \frac{C_{wet}\epsilon}{\sqrt{1-\beta^4}} \frac{\pi d^2}{4} \sqrt{2\rho_{1,g}\Delta p_{tp}} \quad (12)$$

Note:  $\Delta p_{tp}$  = two-phase pressure drops

## Typical Parameters Used in WGM Area

The moisture content of gas flow is crucial for identifying wet gas, with liquid content significantly affecting measurement. The LMP, denoted as X (Tutuianu, 2015), is used to define the wetness or liquid loading of the gas, representing the liquid fraction of a wet gas stream. Equations (13) to (15) show how to calculate the LMP (ASME, 2008).

$$X = \frac{Fr_l}{Fr_g} = \frac{\sqrt{\frac{\Delta P_l}{\Delta P_g}}}{\sqrt{\frac{\rho_g}{\rho_l}}} = \frac{m_l}{m_g} \sqrt{\frac{\rho_g}{\rho_l}} = \frac{Q_l}{Q_g} \sqrt{\frac{\rho_l}{\rho_g}} \quad (13)$$

$$X = \frac{1-GVF}{GVF} \sqrt{\frac{\rho_l}{\rho_g}} = \frac{(1-x)}{x} \sqrt{\frac{\rho_g}{\rho_l}} \quad (14)$$

Where:

$$x = \frac{mg}{mg+ml} \quad (15)$$

The flow of gases and liquids with a LMP ranges from 0 to 0.3, with single-phase flow when X equals 0, and multiphase flow when X exceeds 0.3. Actual gas and liquid mass flow rates can be estimated. Equations (16) and (17) depicts the computation of actual gas and liquid mass flow rates, and the liquid mass flow rate, respectively. Likewise, the gas densimetric Froude number,  $Fr_g$ , is a variant of the standard Froude number,  $Fr$ , applicable to WGF (ASME, 2008) as shown by equation (18). The simplified values are in equations (19) and (20). From equation (20),  $v_{sg}$  is the superficial gas flow average velocity and A = area of the meter inlet. Additionally, equation (21) depicts the gas-to-liquid density ratio.

$$Q_{mg} = \rho_g u_{sg} A \quad (16)$$

$$Q_{ml} = \rho_l u_{sl} A \quad (17)$$

$$Fr_g = \sqrt{\frac{\text{Superficial Gas Inertia Force}}{\text{Liquid Gravity Force}}} \quad (18)$$

$$Fr_g = \frac{v_{sg}}{\sqrt{gD}} \sqrt{\frac{\rho_g}{\rho_l - \rho_g}} \quad (19)$$

$$v_{sg} = \frac{m_g}{\rho_g A} \quad (20)$$

$$DR = \frac{\rho_{l,gas}}{\rho_{liq}} \quad (21)$$

### Vertical WGF Regimes

Two-phase vertical flow has major flow regimes: annular mist, transition, slug-annular, and bubble flow. Slug flow is a

grown bubble with high liquid dominance; transition flow marks the transition from liquid to gas phase, and annular-mist flow is a continuous gas phase with liquid film and droplets (ISO/TR 12748, 2015). Despite these flow patterns, it is not easy to distinguish between flow patterns in two-phase flow because the flow is often in continuous transition. It is assumed to have a large flow velocity (around 10m/s), and the annular flow is the most flow in vertical WGF.

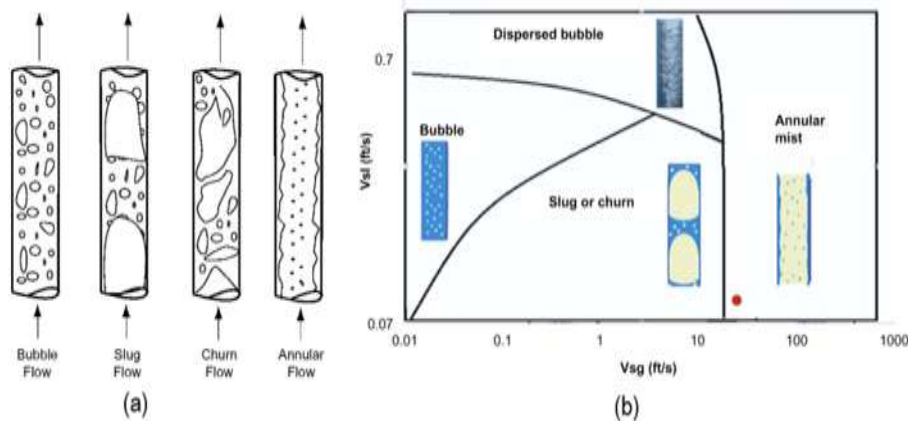


**Figure 3: (a)The vertical WGF regime (ASME, 2008; ISO/TR 12748, 2015) and (b) The exhibition of a two-phase flow map**

### WGM Correlations

Various methods have been used to address over-reading in WGM, with most studies focusing on horizontally installed differential pressure meters. Chisholm and Murdock correlations, developed using an orifice meter, serve as a starting point for a more convenient correlation. In testing the over-reading correlations for Vertical Venturi Wet Gas Meters, a study at NEL showed a homogeneous model with 0.4% accuracy, but improved conditions led to a  $\pm 3\%$  gas mass flow rate error (Graham et al., 2020). Recent research explores the ISO 11583 correlation on vertically installed Venturi (Chinello et al., 2019; Graham et al., 2020). Overreading in Venturi tubes is not significantly

influenced by gas Froude number but largely by line pressure (Chinello et al., 2019). Through that research, it was confirmed that the ISO/TR 11583 over-reading correlation should not be applied directly for vertical Venturi tubes. The list of correlations for WGM is shown in Appendix 1.

### MATERIALS AND METHODS

The study used experimental data from Cranfield University Process System Engineering Lab's annular gas-water two-phase venturi vertical flow loop, describing the setup, instrumentation, and developed a model for estimating pressure drop. It also provided an overview of data processing procedures and tools.

The air-water flow metering test rig consists of three sections: fluid supply and metering, test section, and fluid separation section. It uses a 2-in pipe and a flow loop of 27,000 mm, with a wire mesh sensor for void fraction distribution. Fluid separation occurs after venturi tube exiting the venturi tube. The serpent flow facility uses various instruments and sensors to measure various parameters, including gas flow rate, static pressure, void fraction distribution, and temperature. The key parameter is the apparent flow rate of gas, which is measured using a venturi meter influenced by pressure drop. The Gamma densitometer detector determines void fraction distribution in the throat area. Other measured parameters include flow rates of gas and water, upstream horizontal void fraction, temperature, and pressure. Figure 4 depicts a schematic serpent rig of the experiments.

### Pressure Drop Modelling for Wet Gas

### Vertical Venturi Tube

FM utilizing conventional methods (D.P. measurement) relies on the differential pressure between the tapping locations. According to Equation (2.12), the two-phase mass flow rate is as  $Q_{mgs} = A\sqrt{2\rho_{1,g}\sqrt{\Delta p_{tp}}}$ . Consequently, the significant reduction in pressure along a flow line results in a variation in the fluid's flow rate. The height difference between the inlet (p1) and throat (p2) tapping points in vertical FM results in a hydrostatic pressure decrease between these taps (Chinello et al., 2019). Numerous investigations on two-phase gas-liquid flow patterns for industrial applications indicate that annular flow is the predominant regime seen, particularly at elevated gas dynamic pressures (Aliyu et al., 2017; Ribeiro et al., 2021). Consequently, a model was formulated for upward vertical flow of wet gas, distinguished by a liquid layer on the tube wall and a droplet-laden gas phase traversing the tube core (Sawant et al., 2008) (Figure 5).

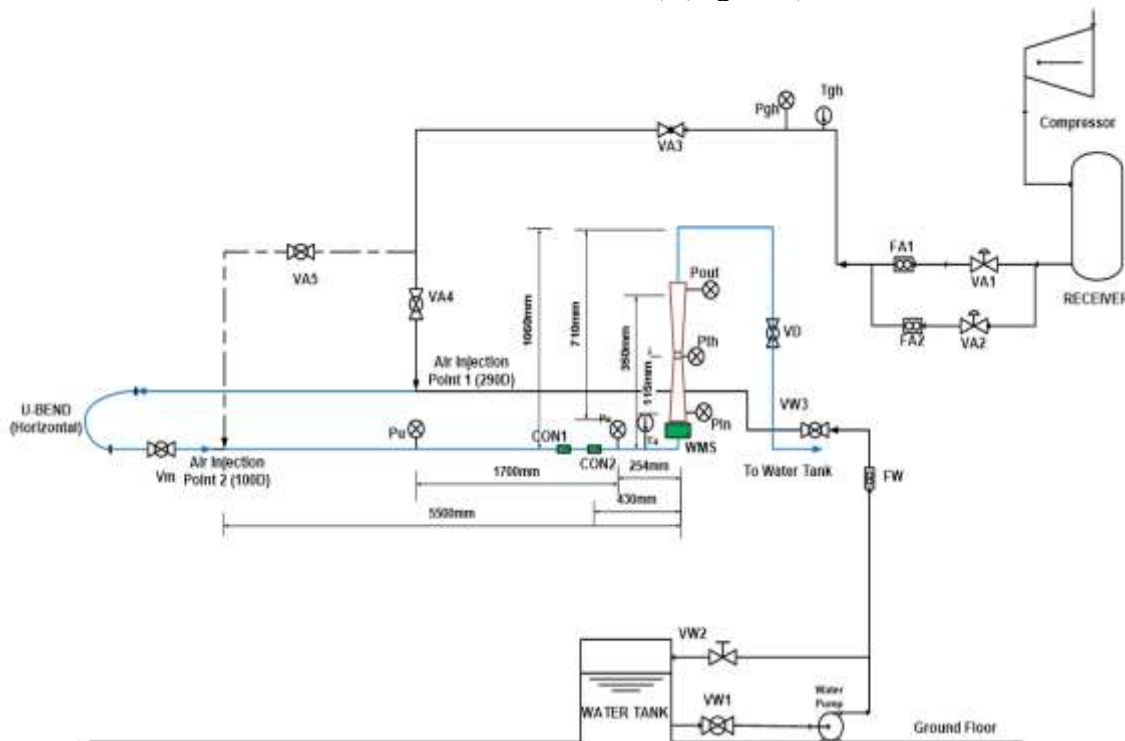
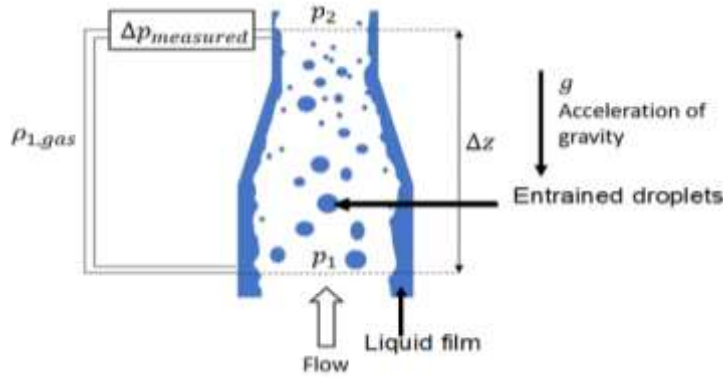


Figure 4: Schematic Serpent Rig



**Figure 5: The diagram illustrates a vertical upward-oriented wet-gas Venturi tube in a schematic representation**

Dry gas flows upward through a venturi meter, with inlet-throat differential pressure expressed as Equation 22, where  $\Delta z$  represents the height difference between pressure taps. Dry gas flows upward through a venturi meter, with inlet-throat differential pressure expressed as Equation 22, where  $\Delta z$  represents the height difference between pressure taps. Likewise, the pressure loss in vertical two-phase WGF is primarily due to hydrostatic pressure, gravitational force effects, and interfacial frictional forces, determined using Equation (24). (25)

$$\Delta p_{measured} = (p_1 - p_2) - \rho_{1,gas} g \Delta z \tag{22}$$

$$p_1 - p_2 = \Delta p_{measured} + \rho_{1,gas} g \Delta z \tag{23}$$

$$\Delta p_{tp} = (p_1 - p_2) - g \Delta z (\rho_{1c,mix} (1 - lff) + \rho_l * lff) \tag{24}$$

Where:

$\Delta p_{tp}$  is the “Two-phase pressure drop,  $p_1$  and  $p_2$  are the Inlet and throat tap pressures, respectively,  $\rho_{1c,mix}$  is the density of the mixed-phase fluid at the core inlet,  $lff$  is the Liquid film fraction, and  $\Delta z$  is the inlet-throat pressure taps differential height”.

It is possible to rewrite Equation (24) in terms of the measured pressure as follows.

$$\Delta p_{tp} = \Delta p_{measured} - g \Delta z (\rho_{1,gas} + \rho_{1c,mix} (1 - lff) + \rho_l * lff)$$

So, in order Equation (25) to fit for mass flow rate computation for vertical orientation,  $\Delta p_{tp}$  is depicted by Equation (24).

**Calculation of the Mixture Density**

The amalgamation of gas and entrained liquid was regarded as being a uniform density ( $\rho_{1c,mix}$ ) in the core zone. The standard density was determined utilizing Equation (26).

$$\rho_{1,mix} = \frac{M_g + M_l}{V_{total}} = \rho_g \alpha_{1c,g} + \rho_l (1 - \alpha_{1c,g}) \tag{26}$$

Where:  $\alpha_{1c,g}$  = core void fraction valued as;

$$\alpha_{1c,g} = \frac{\alpha_{1,g}}{\alpha_{1,g} + \gamma(1 - \alpha_{1,g})} \tag{27}$$

$\alpha_{1,g}$  represents the cross-sectionally averaged void fraction, while  $\gamma$  denotes the droplet holdup, which can be approximated as the entrained droplet fraction,  $e$ .  $M_g$  and  $M_l$  signify the mass of the gas and the mass of the liquid, respectively.  $V_{total}$  indicates the total volume of a specific pipe section, and  $\alpha_{1c,g}$  refers to the gas void fraction at the core of the pipe.

$$\alpha_{1,g} = \frac{A_{1,g}}{A} \tag{28}$$

With  $A_{1,g}$ ,  $g$  representing the cross-sectional area which is filled by the gas.  $A$

= the cross-sectional area of the pipe. The void fraction can be estimated using the Gas Volume Fraction (GVF) as per Equation (29) if the liquid and gas velocities are similar.

$$GVF = \frac{\alpha_{1,g}}{\alpha_{1,g} + \frac{V_l}{V_g}(1 - \alpha_{1,g})} \quad (29)$$

Hence,

$$\rho_{1,mix} = \rho_{1,g}GVF + \rho_l(1 - GVF) \quad (30)$$

The methodology proceeded by approximating the Liquid Film Thickness, Liquid Film Fraction and Entrained Droplet Fraction. Thus, the entrainment rate (e) is a nuanced and complex measure used to assess the pressure decrease of annular two-phase flow. It denotes the ratio of the mass flow rate of entrained droplets to the total liquid (Sawant et al., 2008). Multiple methodologies have been established to assess the value of the entrainment rate. The studies contributing to the creation of correlations in this area are Assad et al. (1998) and Schadel et al. (1990). This work utilizes the mathematical model created by Sawant et al. (2008) as delineated in Equations (31) to (36).

$$e = e_m \tanh(aWe_e^{1.25}) \quad (31)$$

$$We_e = \frac{\rho_g u_{sg}^2}{\sigma} \left( \frac{\rho_l - \rho_g}{\rho_g} \right)^{0.25} \quad (32)$$

$$e_m = 1 - \left( \frac{Re_{lc}}{Re_l} \right) \quad (33)$$

$$Re_l = \frac{\rho_l u_{sl} D}{\mu_l} \quad (34)$$

$$Re_{lc} = 250 \ln(Re_l) - 1265 \quad (35)$$

$$a = 2.31 \times 10^{-4} Re_l^{-0.35} \quad (36)$$

In this context, *a* represents the empirical coefficient, and *We* denote the modified gas Weber number.  $\mu_l$ ,  $\rho_l$  and  $\rho_g$ , are liquid dynamic viscosity, liquid density, and gas density, respectively.

$\sigma$  denotes the liquid surface tension, whereas  $u_{sl}$  and  $u_{sg}$  signify superficial liquid velocity at the local point and the superficial gas velocity, respectively.  $Re_{lc}$  defines the critical Reynolds number for liquids. For that case, when the  $Re_l$  is below  $Re_{lc}$  this means that there is no means of generating entrained droplets (Aliyu et al., 2017).

$$\dot{m}_l = \dot{m}_{lf} + \dot{m}_e \quad (37)$$

Also, “e” when represented via the mass flows, it is as:

$$e = \frac{\dot{m}_e}{\dot{m}_l} = \frac{\dot{m}_l - \dot{m}_{lf}}{\dot{m}_l} \quad (38)$$

Whereby,  $\dot{m}_{lf}$ ,  $\dot{m}_l$ ,  $\dot{m}_e$ , represent the liquid film flow rate in kg/s, total liquid flow rate, and entrained droplet mass flow rate, respectively (Aliyu et al., 2017).

So,

$$\dot{m}_l = \rho_l u_{sl} A_{pipe} = \rho_l u_{sl} \frac{\pi D^2}{4} \quad (39)$$

And

$$\dot{m}_{lf} = \rho_l u_{lf} A_{lf} = \rho_l u_{lf} (D - \delta) = (1 - e) \dot{m}_l \quad (40)$$

The liquid film fraction (lff) denotes the ratio of the liquid film along the pipe walls to the total liquid volume in the fluid flow, represented as  $1 - e$ .

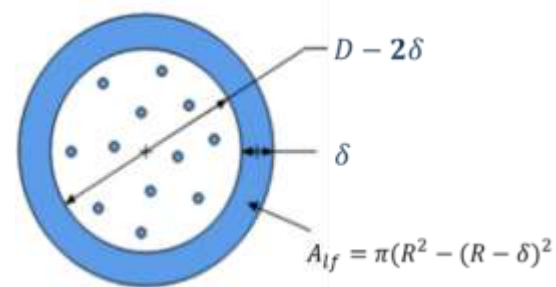


**Figure 6: Liquid mass balance demonstrating the droplets and film when occupying the studied pipe**

*Source: Aliyu et al. (2017)*

According to Equation (40), the area filled by the liquid film,  $A_{lf}$ , is derived from Equation (41), while the average liquid film velocity,  $U_{lf}$ , is calculated using Equations

(42) and (43), under the assumption of fully developed flow with cross-sectionally axis-symmetric characteristics (Aliyu et al., 2017).

$$A_{lf} = \pi(R^2 - (R - \delta)^2) \quad (41)$$

$$u_{lf} = \frac{\dot{m}_{lf}}{A_{lf}\rho_l} \quad (42)$$

$$u_{lf} = \frac{u_{sl}D^2(1-e)}{4t(D-\delta)} \quad (43)$$

whereby,  $D$ ,  $u_{sl}$ ,  $u_{lf}$ ,  $\delta$ , and  $e$  = pipe internal diameter, liquid superficial velocity, measured film velocity, measured film thickness, and entrained liquid fraction, respectively.

### The Liquid Film Thicknesses

Liquid film thickness is the height of the liquid layer uniformly spread around a Venturi pipe (Wang et al., 2020), requiring entrainment rate, gas velocity, and liquid film boundary layer. Estimating this requires a conductance probe with an error margin of  $\pm 3\%$  (Aliyu et al., 2017). However, mathematical models can provide an approximate outcome (equations 44 to 46). Henstock's mathematical approach was effective for estimating vertical annular flow sheet thickness, but not suitable for downhill flow rig configurations. Likewise, Okawa et al. (2001) proposed a model (equation 47) for estimating liquid film thickness by balancing interfacial shear force and wall friction force, based on the rate of droplet entrainment (Berna et al., 2014).

$$\frac{\delta}{D} = \frac{6.95F}{(1+1400F)^{0.5}} \quad (44)$$

$$F = K \left(\frac{v_l}{v_g}\right) \left(\frac{\rho_l}{\rho_g}\right)^{0.5} Re_g^{-0.9} \quad (45)$$

$$K = [(0.707Re_l^{0.5})^{2.5} + (0.0379Re_l^{0.9})^{2.5}]^{0.4} \quad (46)$$

$$\delta = \frac{1}{4} \sqrt{\frac{f_w \rho_l u_{lf}}{f_{gi} \rho_g u_g}} D \quad (47)$$

In Equation (3.26), the wall friction factor, denoted as  $f_w$  is defined as  $\max(\frac{16}{Re_{lf}}, 0.005)$  represents the ‘‘Reynolds number’’ of the liquid in the layer’s wall, as indicated in Equation (3.27), and,  $f_{gi}$  is the interfacial friction factor specified by equation 48. Equation (49) demonstrated a relationship on predicting liquid film (Ishii & Grolmes, 1975).

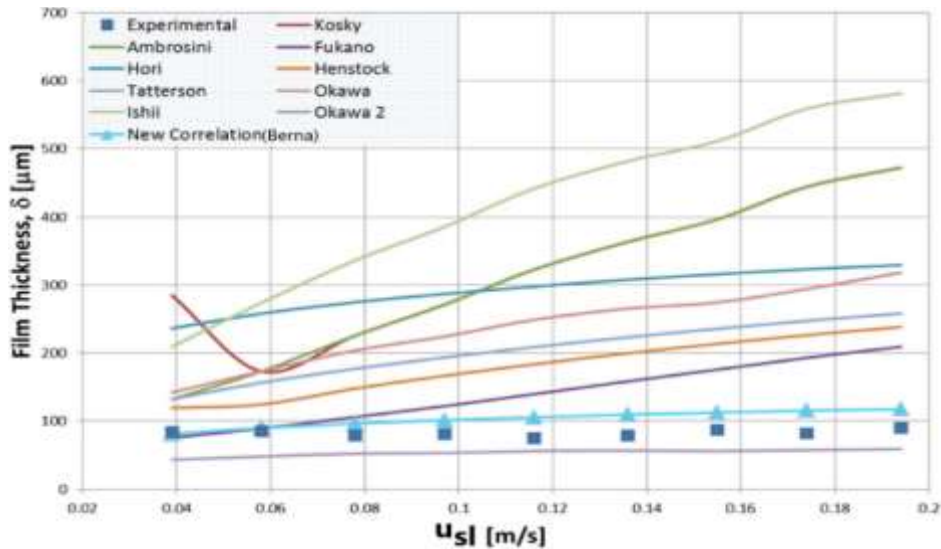
$$Re_{lf} = \frac{4m_{lf}}{\mu_l P} = \frac{4\rho_l u_{lf} \delta}{\mu_l} \quad (48)$$

$$f_{gi} = fg(1 + 300 \frac{\delta}{D}) \quad (49)$$

$$\delta = 0.347 Re_{lf}^{2/3} \sqrt{\frac{\rho_l \mu_l}{\tau_l \rho_l}} \quad (50)$$

Equation (50) evaluates the equilibrium that occurs when there is a drag force exerted by the gas on the wave in the film (Berna et al., 2014). The association is delineated in equation 51. The performance model for film thickness is found to be an accurate approximation, as its values closely align with experimental data, as shown in Figure 7.

$$\frac{\delta}{D} = 7.165 Re_g^{-1.07} Re_l^{0.48} \left(\frac{Fr_g}{Fr_l}\right)^{0.24} \quad (51)$$



Note: Vertical upward flow,  $D=0.0234$  m, ambient pressure and temperature,  $v_{sg} = 71$  m/s

Source: Berna et al. (2014)

**Figure 7: Analysis of liquid film thickness in relation to superficial liquid velocity based on vertical data of Schubring using the existing correlations.**

The parameters that were utilised for computing air-water wet gas are in Table 1.

**Table 1: Parameters for computing air-water wet gas**

Parameter	Symbol	Value	Unit
Dynamic Viscosity air (at 26°C)	$\mu_g$	1.841E-05	Ns/m <sup>2</sup>
Dynamic viscosity of water (at 26°C)	$\mu_l$	0.0008693	Ns/m <sup>2</sup>
Water density	$\rho_l$	996.8	kg/m <sup>3</sup>
Pipe Diameter	D	0.0548	m
Gas density (at 20°C, 1barg)	$\rho_g$	1.209	kg/m <sup>3</sup>
Throat Diameter	d	0.0274	m
Superficial Reynold number	$Re_l$	10921.312	-
Critical Superficial Reynold number	$Re_{lc}$	1059.6179	-
Maximum entrainment	$e_m$	0.9029771	-
Surface tension	$\sigma_l$	0.07199	N/m
Empirical coefficient	a	8.917E-06	-
Liquid Mass Flow Rate	$m_l$	0.4086156	kg/s
Kinematic Viscosity of liquid	$\nu_l$	8.7E-07	m <sup>2</sup> /s
Kinematic Viscosity of air	$\nu_a$	15.61	m <sup>2</sup> /s
Acceleration due to gravity	$to$	9.81	N/m <sup>2</sup>
Differential height	$\Delta z$	0.11502	m
Discharge Coefficient	Cd	0.995	-
Throat Area	$A_{th}$	0.0005896	m <sup>2</sup>
Density Ratio (at 20°C)	DR	0.0012129	-
Average Temperature	T	24.894032	-
Expansibility ratio (wet gas)	$\epsilon_{wet}$	0.93	-

Approach velocity factor	E	1.0327956	-
Beta Ratio	$\beta$	0.5	-
Expansibility ratio (dry gas)	$\epsilon$	0.994236	-
Pipe Area	$A_{\text{pipe}}$	0.0023586	m <sup>2</sup>
Pipe Radius	R	0.0274	m

## RESULTS AND DISCUSSION

### Comparison of Reference and Expected Gas Mass Flowrates

The computed reference wet gas mass flow rate ( $Q_{mg}$ ) varies from 0.0645 kg/s to 0.0676 kg/s, exhibiting a narrow range due to minor fluctuations in inlet pressure gas surface velocity and upstream gas density ( $\rho-1g$ ).  $Q_{mg}$  presumes ideal gas behaviour under frictionless and incompressible flow circumstances. WGF results show that a hydrostatic pressure drop affects liquid content flow, with pipe pressure decreasing and not offset by impulse line pressure drop. Different values of discharge and

compressibility constants compensate. Figure 9 illustrates the correlation between the flow rates. The equations' slopes represent the average ratio of the observed gas mass flow rate to the  $Q_{mg}$ , which is the mean over-reading. A steeper slope indicates greater over-reading, resulting in reduced accuracy; conversely, a shallower slope signifies improved accuracy. The estimated gas flow rate derived from the coefficient of discharge in the ISO/TR11583 correlation, utilizing a slope of 10.133 as directly obtained from the equation, is firstly presumed accurately.

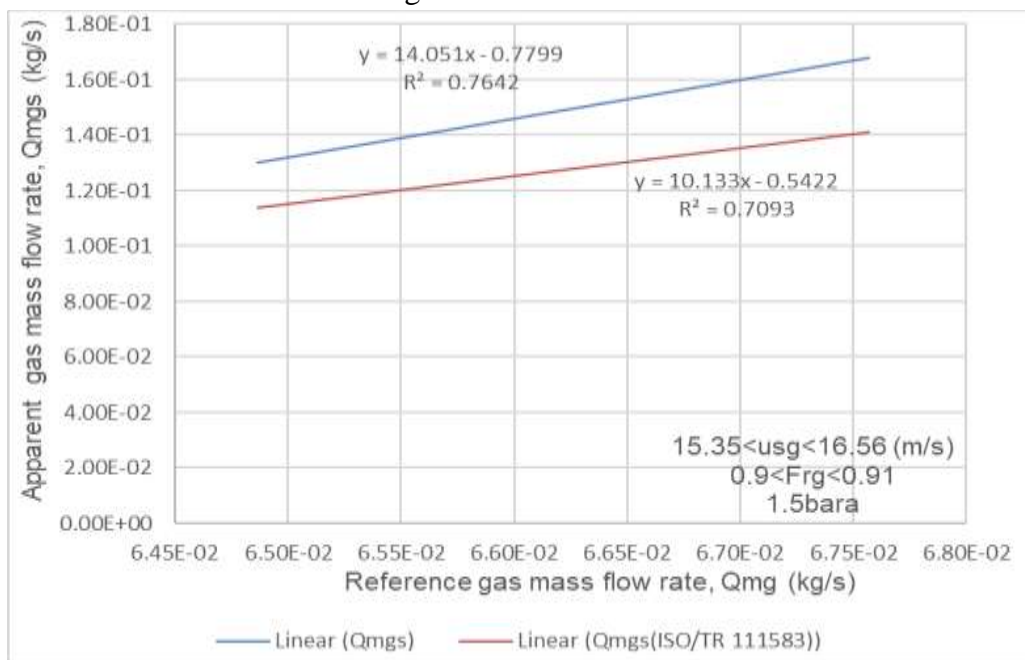


**Figure 8: Comparing  $Q_{mg}$  and  $Q_{mgs}$  (ISO/TR11583)**

### Comparing the over-reading values vs LMP

The over-reading outcomes of Homogeneous, De Leeuw, and ISO/TR 11583 correlations for two-phase air-water

flow are influenced by input parameters, with n-exponential value affecting Chisholm constant, with 0.5 n-exponential value yielding the highest results (Figure 9).

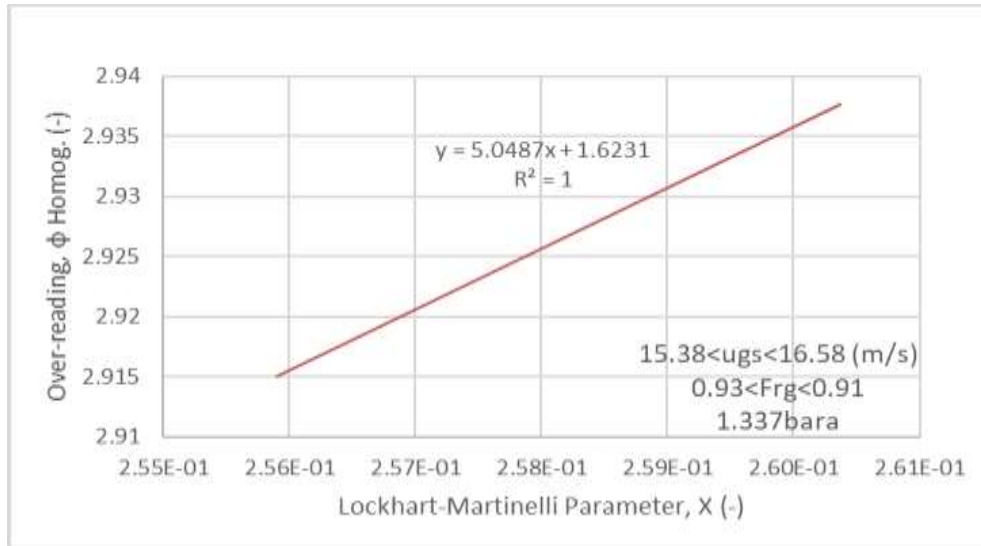


**Figure 9: Comparing the over-reading values vs LMP**

The De Leeuw correlation provides two possibilities for exponential n-exponential values, with the selected n value being 0.41. Figure 10 shows the over-reading values for De Leeuw varied from 2.262 to 2.281, exhibiting a range of 0.0019. The ISO/TR 11583 correlation was influenced by n-exponential, discharge coefficient (C), and H-value parameters. The n-exponential value was 0.347, and the discharge coefficient was 0.964, resulting in the lowest over-reading results among the three correlations. However, the H-value was assumed to be 1.35 due to the pure water

phase. The ISO/TR 11583 model's over-reading values ranged from 1.93 to 1.9463, with a range of 0.0148. The analysis of variations in over-reading values revealed the interdependence of these values with the LMP. The plot in Figure 10 shows a positive linear representation with an r-squared value of 1, indicating a perfect correlation between the two variables. Over-reading results typically increase with liquid content increase from 0 to 5 percentage LVF or within the Lockhart Martinelli parameter range.

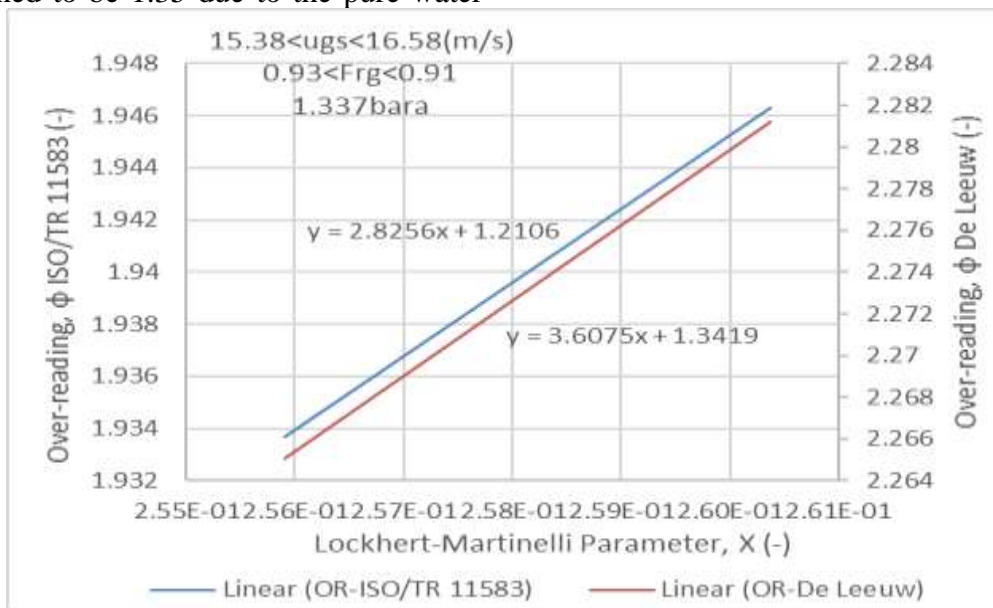


**Figure 10: LMP versus Over-reading values**

**Performance of the over-reading relationships**

The performance of the three adjustments' over-reading was assessed by calculating the projected gas flow rate deviation from the actual value. The relative percentage inaccuracy in gas flow was calculated using Equation (52).

$$\phi_{RE}(\%) = \left( \frac{\phi_{mg\_cor} - \phi_{mg\_actual}}{\phi_{mg\_actual}} \right) \times 100 \tag{52}$$

Where:  $\phi_{g\_cor}$  denotes the over-reading value of the correlation, and  $\phi_{g\_actual}$  represents the reference or actual over-reading. Figure 11 depicts the relative errors which were depicted against the LMP.

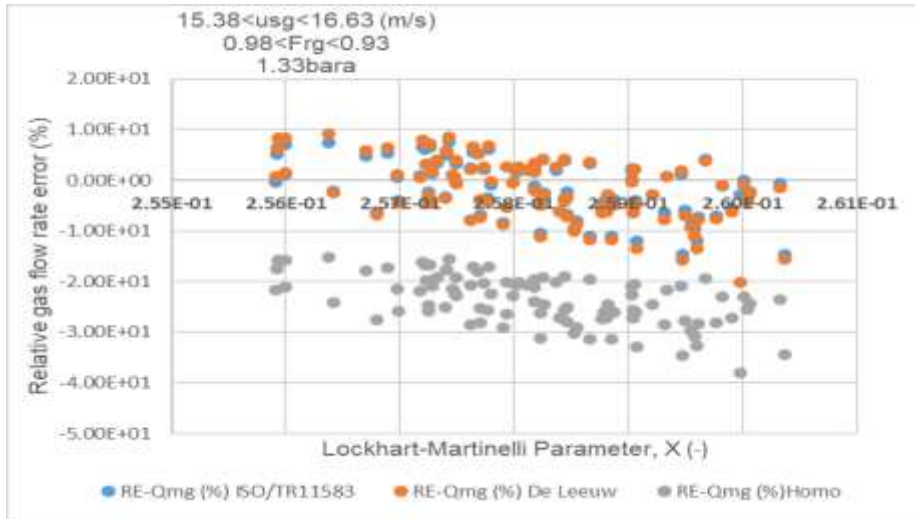


**Figure 11: A plot demonstrating X parameter versus the relative gas flow rate errors (%)**

Standardized correlation has a cluster of points with relative errors from 10 to 40 percentage, primarily due to the approximation of the exponential n value. This approximation compensates for source pressure drop, causing inaccuracies in FM.

Reducing the n value to below 0.5 enhances the model, resulting in a smaller error. Assuming n equals 0.4, the relative error is  $\pm 10\%$ .

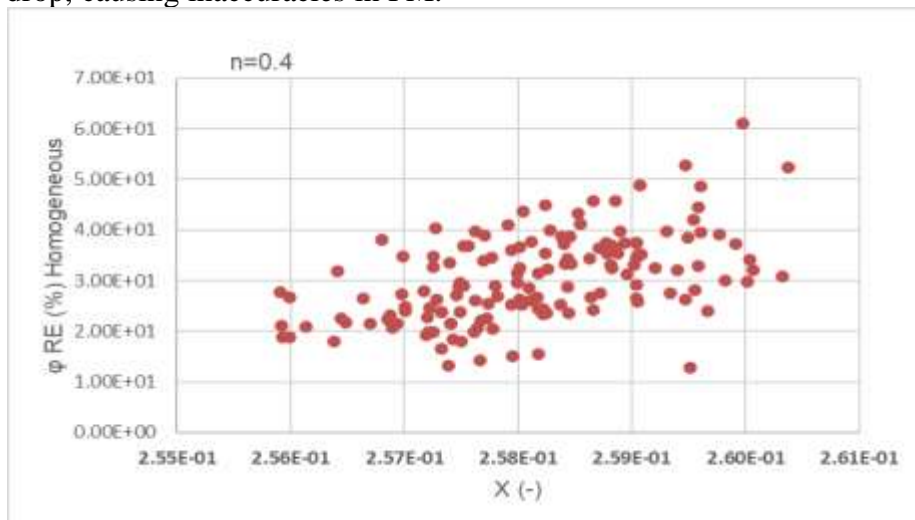


**Figure 12: Assessing the influence of Homogeneous correlation when n is 0.4**

De Leeuw and ISO/TR11583's over-reading correlations errors are closely linked to their range, with a relative inaccuracy estimated to be around  $\pm 10$  (Figure 10). De Leeuw and ISO/TR11583's over-reading correlations errors are closely linked to their range, with a relative inaccuracy estimated to be around  $\pm 10$ . To specify their error value more precisely, the statistical approach is employed to calculate the root mean square of the relative error for each correlation equation

$$RMS = \sqrt{\frac{1}{N} \sum_{i=1}^N \left( \frac{\phi_{g\_cor} - \phi_{g\_actual}}{\phi_{g\_actual}} \right)^2} \quad (53)$$

RMS denotes the Root Mean Square of the over-reading relative error, while N represents the sample size or the number of data points collected. In this instance, 200 data points were analyzed, and computations were performed to yield the results displayed in Table 2. From it, the ISO/TR11583 correlation has an RMS error of 6.35%, making it the most effective of the three correlations analyzed, albeit its substantial RMS.

**Table 1 Comparing various relative errors**

Correlation	Statistical results based on the comparison		
	Homogeneous	De Leeuw	ISO/TR 11583
RE Mean Square	0.09.69	0.0051	0.00403
RE Max Square	0.375	0.06.38	0.0564
RE Root Mean Square (RMS)	0.311336	0.0714	0.063456
Standard Deviation	0.058388	0.007638	0.005817
RMS (%)	3.11	7.14	6.35

**Variation of Over-reading and Gas Froude Number with Gas Wetness**

As a function of the gas's surface velocity, the Gas Froude number is a critical metric for evaluation in WGM. The value was

calculated using Equation (2.22), and the findings are illustrated in a composite graph depicting the over-reading of ISO/TR11583 about the LMP (X).

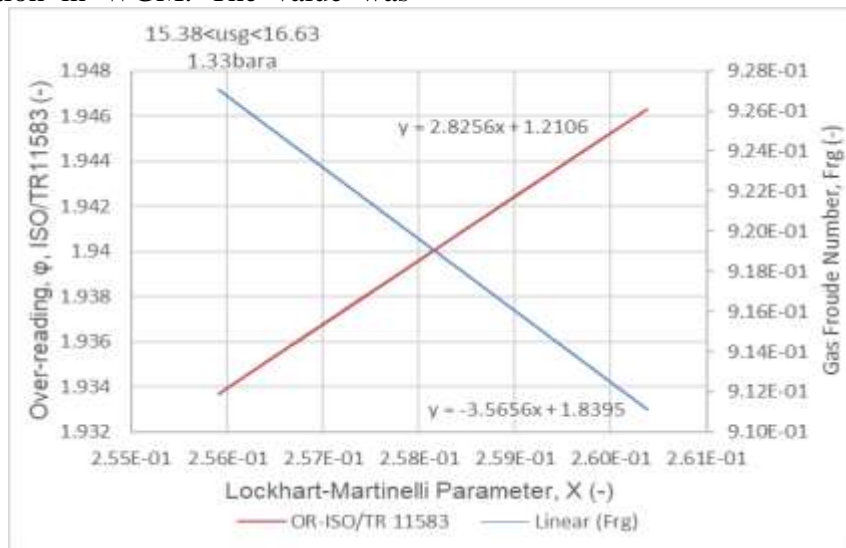


**Figure 13: Comparing the associations between the over-reading gas Froude number as per LMP and ISO/TR11583**

Figure 13 illustrates an inverse correlation between the gas Froude number and over-reading data, where the maximum Froude number corresponds to diminished over-

reading values. This relationship is precisely proportional to the gas's superficial velocity, signifying that over-reading diminishes as the gas's superficial

velocity increases. The graph illustrates a correlation between the Froude number and the LMP, demonstrating that values for X rise as the Froude number diminishes. This indicates that utilizing high velocity in wet gas is warranted, as the presence of liquid diminishes the gas's surface velocity.

### The correlation between Gas Froude

### Number and Entrainment Rate

The entrainment rate ( $e$ ) is a crucial factor in pipe flow, indicating the volume of liquid entrained. The study uses equations (3.10) to (3.15) from Sawant et al. (2008) to approximate entrainment rate values, highlighting the significant correlation between entrainment rate and gas Froude number (Figure 4-7).

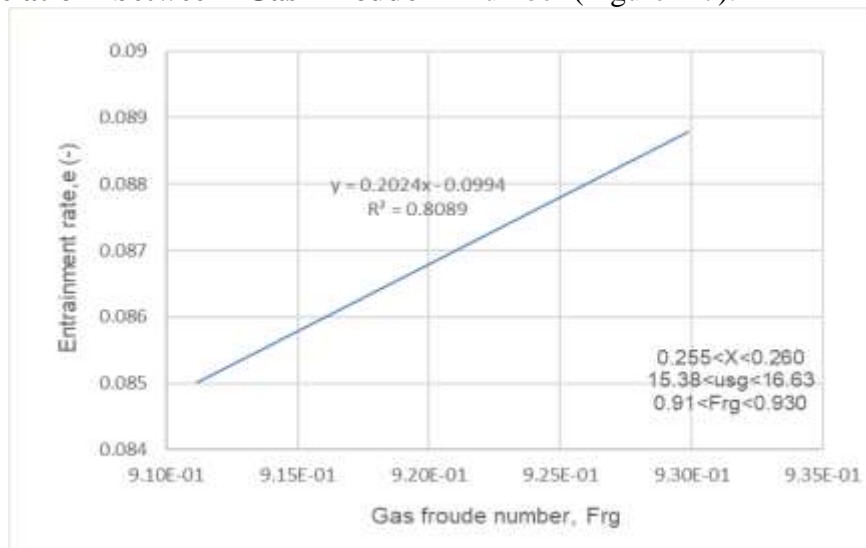


**Figure 14: Estimating the relationship between gas Froude number and entrainment rate**

Within the Lockhart-Martinelli range of 0.255 to 0.26, Figure 14 illustrates that the Froude number is exactly proportional to the entrainment rate. An increase in the surface velocity of gas leads the liquid film layer along the pipe to detach as droplets, rendering the core practically hazy. The reduction in the liquid film enhances the flow, henceforth diminishing the over-reading value. Consequently, the analysis indicates that the rise in entrainment rate is attributable to an upsurge in velocity, leading to a reduction in the overestimation of the moist gas flow.

The validation of outcomes has been accomplished by considering two cases. Initially, a survey was conducted comparing this study with prior research under analogous conditions to assess its concordance with existing findings. Secondly, various data resembling wet gas (but not actual wet gas) have been

evaluated to examine the trend of the results and compare them with the study. Moreover, prior research (Chinello, 2019; Graham et al., 2014) has rectified the inaccuracies in wet gas over-read correlations by employing the exponential-n fitting method. This study evaluates the applicability of the earlier proposed models and ultimately does Excel n-fitting to identify the most effective method for correcting over-reading errors.

The outcomes were verified by conducting an experiment at NEL for vertical venturi wet gas measurements. The experiment utilized a Venturi tube,  $\beta=0.6$ , 4-inch, tested across several wet-gas conditions (Graham et al., 2014). The evaluated D.R values were 0.023, 0.046, and 0.083, while the gas Froude number ranged from 1.5 to 5.5. Figure 15 depicts the anticipated over-readings for such an experiment.

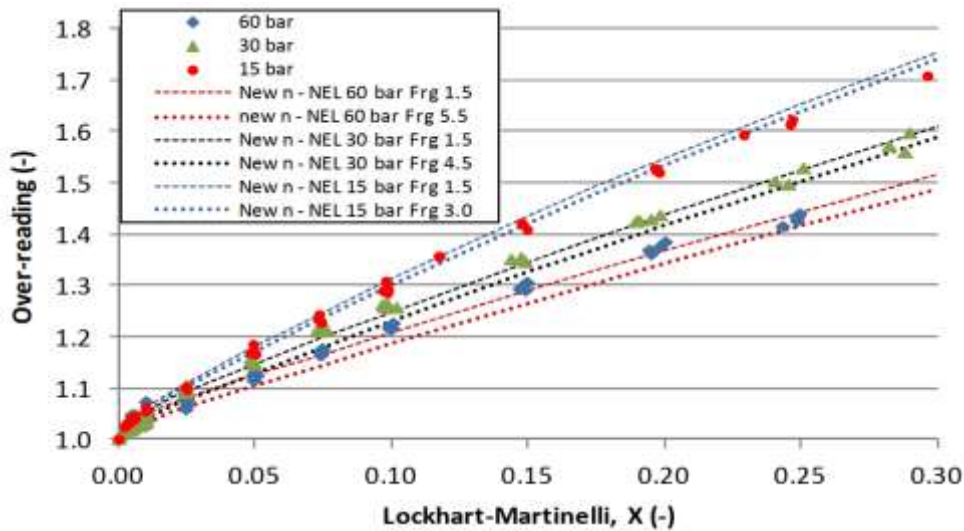


**Figure 15: Forecasting gas Froude numbers and pressure variations as the data from Venturi tube tests**

Figure 16 illustrates the correlation between the anticipated over-reading and X, considering the variations of pressure and gas Froude numbers. The graphs indicate that when pressure diminishes, the slope of the trending lines escalates. The elevation in pressure results in an

augmentation of over-read concomitant with a reduction in X. The results of the fluctuation of differential pressure about over-reading and X obtained at NEL are analogous to the yield of this study (Figure 16).

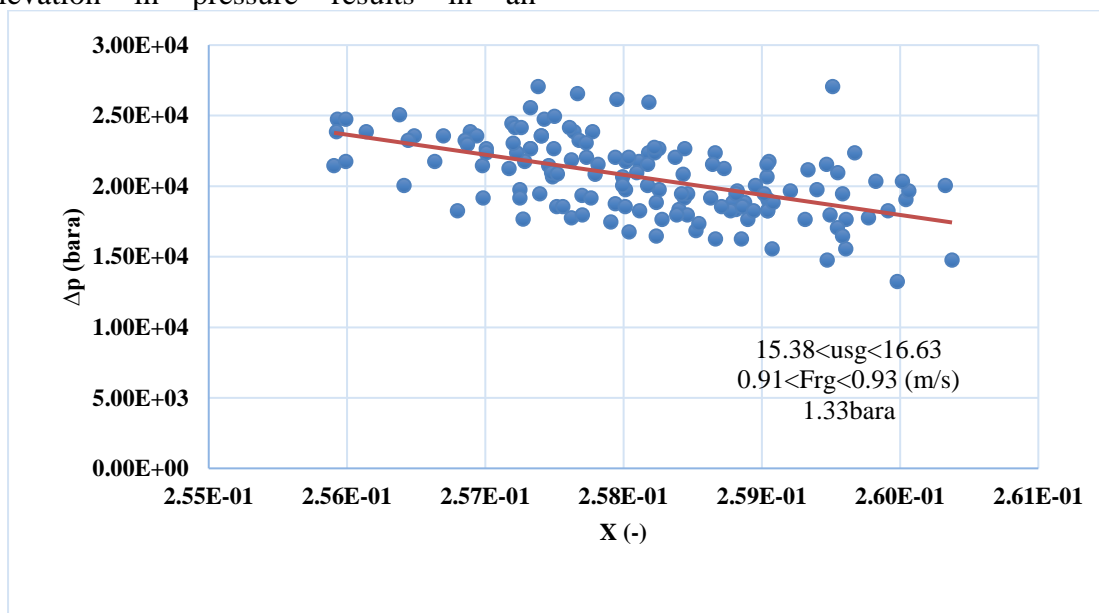


**Figure 16: Differences between the LMP and differential pressure**

This assumption implies a connection between the range of over-reading values observed in the NEL experiment and those identified in this investigation. If the NEL experiment were conducted at lower pressure (0-1.5 bara), the over-reading at

X=2.5 would exceed 1.8, corresponding to this study's findings. Figure 17 shows the results for the de Leeuw and NEL correlations.

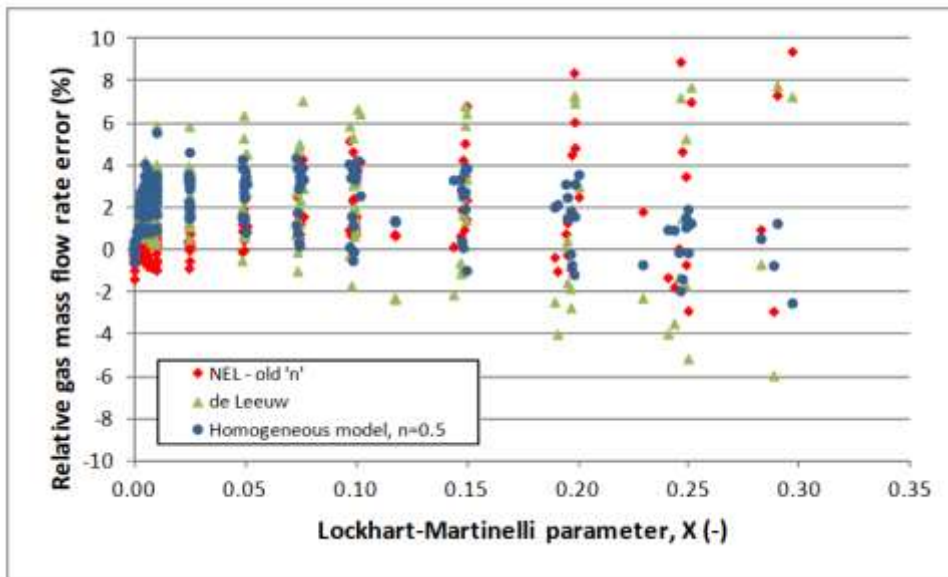


**Figure 17: The de Leeuw and NEL correlations**

Figure 18 illustrates the distribution in NEL, when employing the original exponential “n” as utilized in this investigation. The data values before fitting were outside the ISO/TR11583 standard’s ±3% tolerance, but both investigations

showed a maximum relative error of less than 10%. This pattern was also demonstrated by Chinello (2019) using a Venturi tube at Glasgow Caledonian University. The exponential n was derived from data fitting.

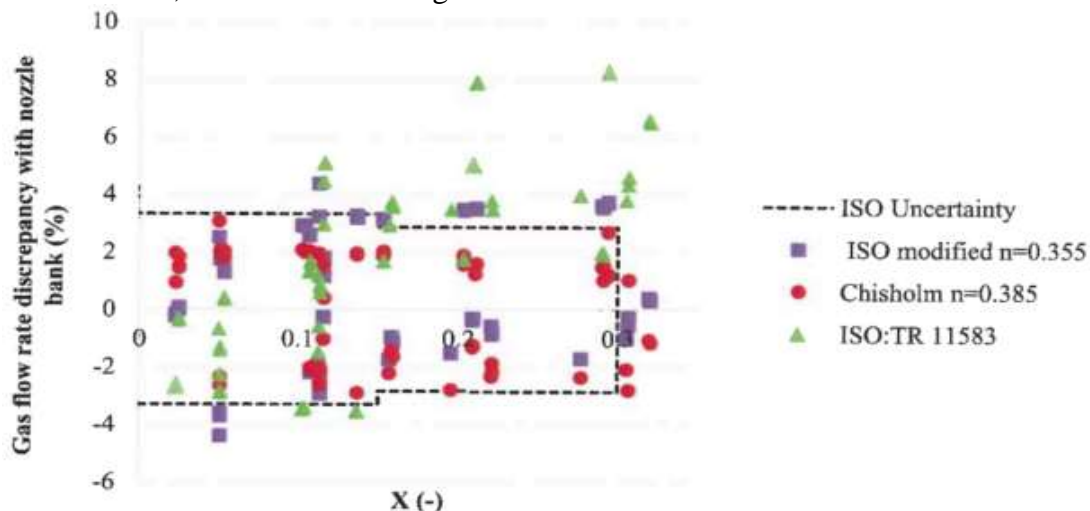


**Figure 18: The vertical Venturi tube in WGF had a divergence in gas mass flow rate with the reference nozzle bank, which was corrected using various correlations, including Chisholm-type correlation (n=0.385) and the ISO/TR 11583 correlation (n=0.355)**

**Existing Correction Techniques for Measurement Improvement**

The study found that current correlations for wet gas over-reading correction with a vertical venturi meter are less effective than those performed horizontally. The determinant of the over-reading value is the n-exponent in computing Chisholm’s

constant, and n-exponential fitting is the primary method for error reduction (Graham et al., 2014).

In the NEL experimental configuration of this study, Graham et al. (2014) established the dependence of n on the density ratio. Equation (54) can be applied to estimate the

value of the n-exponent via an arithmetic model.

$$n = 0.5 - 0.00283(DR^{-0.75} - 1) \quad (54)$$

Chinello (2019) discovered an equation for n-exponential fitting under low-pressure and high-pressure situations in his experiment at GCU.

$$n = 0.65(DR)^{0.097} \quad (55)$$

The efficacy of the proposed equations was evaluated using the WGF from this

investigation, and their impact on error reduction was noticed.

Figure 19 depicts the results which were found, and it shows that altering Chinello's equation by changing the n-exponential from 0.347 to 0.351 did not improve the RMS error in over-reading for ISO/TR11583 correlation but increased the error margin to 29.5%, proving ineffective.

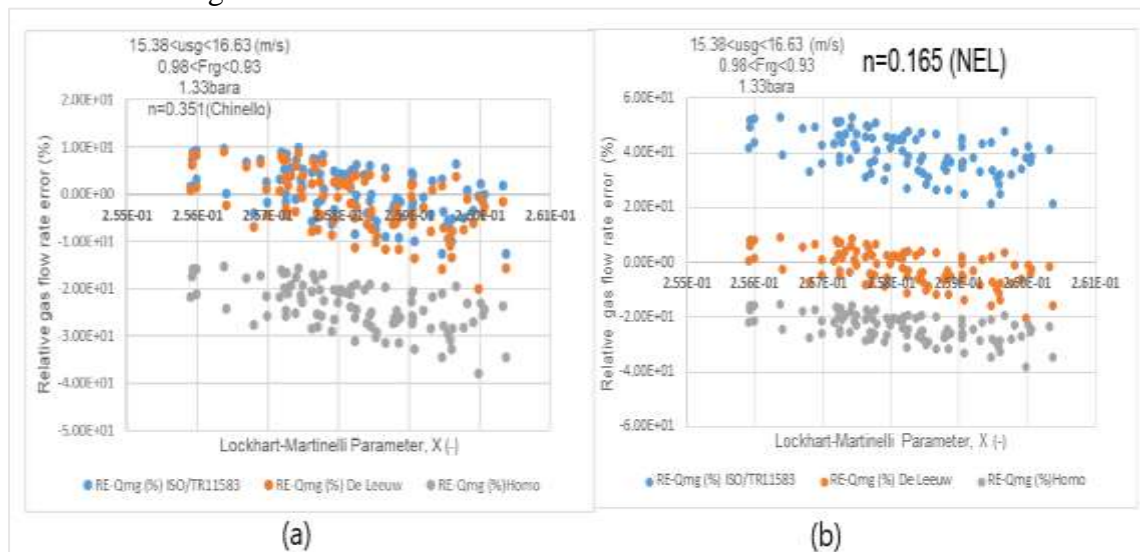


**Figure 19: Difference of % versus X parameter to evaluate n-exponential fitting performance for wet gas vertical venturi flow metering when (a) n is 0.351: Chinello’s equation and (b) when n is 0.165: NEL’s equation**

## CONCLUSION

This study aims to improve WGM technology by using a vertically placed venturi flow meter as the measurement instrument. The existing relationships are based on horizontal alignment, but optimal flow outcomes require vertical installation. The study aims to improve horizontal WGF correlation with vertical WGF using connections like Homogeneous, De Leeuw, and ISO11583. The pressure drop model for annular wet gas vertical flow is proposed to identify over-readings and compare results with established correlations. The study used Cranfield University PSE Lab data, showing ISO/TR11583 correlations have nearly identical performance at reduced intake

pressure, but with a superior RMS error of 6.25%. To enhance the coefficients of both correlations, the discharge coefficient and the n-exponent should be revised to address hydrostatic pressure drop requirements. A high superficial gas velocity is advised for enhanced accuracy in upward vertical WGF. However, hydrostatic correction may be disregarded for elevated Froude numbers, as the film tends to dissipate, resulting in approximately entire mixed phase at the core. The inaccuracy observed in this investigation is much higher than the specified *d* range in ISO/TR11583. Error correction was performed via the *n*-fitting method, which should be refined for each application.

## REFERENCES

- Aliyu, A. M., Almagbrok, A. A., Baba, Y. D., Archibong, A. E., Lao, L., Yeung, H., & Kim, K. C. (2017). Prediction of entrained droplet fraction in co-current annular gas–liquid flow in vertical pipes. *Experimental Thermal and Fluid Science*, *85*, 287–304. <https://doi.org/10.1016/j.expthermflusc.2017.03.012>
- Almagbrok, A. A., Aliyu, A. M., Lao, L., & Yeung, H. (2016). Gas/liquid flow behaviours in a downward section of large diameter vertical serpentine pipes. *International Journal of Multiphase Flow*, *78*, 25–43. <https://doi.org/10.1016/j.ijmultiphaseflow.2015.09.012>
- ASME. (2008). *Wet Gas Flowmetering Guideline*.
- Assad, A., Jan, C., Lopez De Bertodano, M., & Beus, S. (1998). Scaled entrainment measurements in ripple-annular flow in a small tube. In *Nuclear Engineering and Design* (Vol. 184).
- Berna, C., Escrivá, A., Muñoz-Cobo, J. L., & Herranz, L. E. (2014). Review of droplet entrainment in annular flow: Interfacial waves and onset of entrainment. In *Progress in Nuclear Energy*, *74*, pp. 14–43. <https://doi.org/10.1016/j.pnucene.2014.01.018>
- Chinello, G. (2019). *Wet gas metering with Venturi tubes*. Ph.D. Thesis, Glasgow Caledonian University, UK.
- Chinello, Graham, E., Reader-Harris, M., Clark, S., & Collins, A. (2019). Using Venturi Meters Installed in Vertical Orientation for Wet-Gas Flow Measurement. *North Sea Flow Measurement Workshop 22-25 October 2019*.
- Chisholm, D. (1977). *Research Note: Two-Phase Flow Through Sharp-Edged Sharp-Edged*. 128–130.
- Collins, A., & Clark, S. (2013). Evolution of wet gas venturi metering and wet gas correction algorithms. In *Measurement and Control, United Kingdom*, *46*(1), pp. 15–20. <https://doi.org/10.1177/002029401304600102>
- Flowmeters. (2015, July). *Differential Pressure Flow Meters (DP Flow Meters)*. <https://www.flowmeters.co.uk/differential-pressure-flow-meters-dp-flow-meters/>
- Graham, E., Michael Reader-Harris, N., David Hodges, N., Richard Hone, N., Amanda Barrie, N., & Neil Ramsay, N. (2014). Performance of a Vertically Installed Venturi Tube in Wet-Gas Conditions. In *32nd International North Sea Flow Measurement*. <https://nfogm.no/wp-content/uploads/2019/02/2014-06-Performance-of-a-Vertically-Installed-Venturi-Tube-in-Wet-Gas-Conditions-Graham-NEL.pdf>
- Graham, Reader-Harris, M., Chinello, G., Harkins, K., Bowman, N., & Wales, L. (2020). Vertically installed Venturi tubes for wet-gas flow measurement: Possible improvements to ISO/TR 11583 to extend its range of applicability. *Flow Measurement and Instrumentation*, *74*. <https://doi.org/10.1016/j.flowmeasinst.2020.101757>
- Graham, Reader-Harris, M., Ramsay, N., Boussouara, T., Forsyth, C., Wales, L., & Rooney, C. (2015). Impact of Using ISO/TR 11583 for a Venturi Tube in 3-Phase Wet-Gas Conditions. In *33rd International North Sea Flow Measurement*.
- Henstock, W., & Hanratty, T. (1976). The interfacial drag and the height of the wall layer in annular flows. *AIChE Journal*, *22*(6), 990–1000. <https://aiche.onlinelibrary.wiley.com/doi/10.1002/aic.690220607>
- Ishii, M., & Grolmes, M. A. (1975). Inception criteria for droplet entrainment in two-phase concurrent film flow. *AIChE Journal*, *21*(2), 308–318.

- ISO5167-04. (2003). *Measurement of fluid flow by means of pressure differential devices inserted in circular cross-section conduits running full-Part 4: Venturi tubes*. <https://www.sis.se/std-903588>
- ISO/TR 11583. (2012). *Measurement of wet gas flow by means of pressure differential devices inserted in circular cross-section conduits*, ISO/TR 11583:2012.
- ISO/TR 12748. (2015). *Natural Gas — Wet gas flow measurement in natural gas operations* (PD ISO/TR 12748:2015). [www.iso.org](http://www.iso.org)
- Liu, X., Lao, L., & Falcone, G. (2020). A comprehensive assessment of correlations for two-phase flow through Venturi tubes. *Journal of Natural Gas Science and Engineering*, 78, 103323. <https://doi.org/10.1016/j.jngse.2020.103323>
- Livelli, G. (2010). *Flowmeter piping requirements*. PI Process Instrumentation. <https://www.piprocessinstrumentation.com/instrumentation/flow-measurement/coriolis/article/15553997/flowmeter-piping-requirements>
- Murdoch, J. W. (1962). *Two-Phase Flow Measurement With Orifices*. [http://asmedigitalcollection.asme.org/fluidsengineering/article-pdf/84/4/419/5569552/419\\_1.pdf](http://asmedigitalcollection.asme.org/fluidsengineering/article-pdf/84/4/419/5569552/419_1.pdf)
- Okawa, T., Kitahara, T., Yoshida, K., Matsumoto, T., & Kataoka, I. (2001). New entrainment rate correlation in annular two-phase flow applicable to wide range of flow condition. *International Journal of Heat and Mass Transfer*, 45. [www.elsevier.com/locate/ijhmt](http://www.elsevier.com/locate/ijhmt)
- Ribeiro, J. X. F., Liao, R., Aliyu, A. M., Ahmed, S. K. B., Baba, Y. D., Almbrok, A. A., Archibong-Eso, A., & Liu, Z. (2021). A Two-Fluid Model for High-Viscosity Upward Annular Flow in Vertical Pipes. *Energies* 2021, 14, 14(12), 3485. <https://doi.org/10.3390/EN14123485>
- Salehi, S.M., Lao, L., Xing, L., Simms, N. and Drahm, W. (2024), “Devices and methods for wet gas flow metering: A comprehensive review”, *Flow Measurement and Instrumentation*, 96, p. 102518, doi: <https://doi.org/10.1016/j.flowmeasinst.2023.102518>.
- Sawant, P., Ishii, M., & Mori, M. (2008). Droplet entrainment correlation in vertical upward co-current annular two-phase flow. *Nuclear Engineering and Design*, 238(6), 1342–1352. <https://doi.org/10.1016/j.nucengdes.2007.10.005>
- Schadel, S. A., Leman, G. W., Binder, J. L., & Hanratty, T. J. (1990). Rates Of Atomization And Deposition In Vertical Annular Flow. *International Journal of Multiphase Flow*, 16(3), 363-374.
- Steven, R. (2001). *Wet Gas Metering*. PhD Thesis, Department of Mechanical Engineering, University of Strathclyde, UK
- Steven, R. N. (2002). Wet gas metering with a horizontally mounted Venturi meter. *Flow Measurement and Instrumentation*, 12(5–6), 361–372. [https://doi.org/10.1016/S0955-5986\(02\)00003-1](https://doi.org/10.1016/S0955-5986(02)00003-1)
- Tutuianu, C. (2015). *An Introduction to Wet-Gas Flow Metering*. National Measurement System, TUV-NEL. [https://www.academia.edu/35673797/good\\_practice\\_guide\\_an\\_introduction\\_to\\_wet\\_gas\\_flow\\_metering](https://www.academia.edu/35673797/good_practice_guide_an_introduction_to_wet_gas_flow_metering)
- Wang, J., Xu, Y., Zhang, T., Wu, H., Wang, H., & Huo, X. (2020). A pressure drop model for the annular-mist flow in vertical Venturi. *Journal of Natural Gas Science and Engineering*, 76. <https://doi.org/10.1016/j.jngse.2020.103168>
- Zhang, Q. and Liu, D. (2019), “Study on

application of wet gas metering technology in shale gas measurement”, *FLOMEKO 2019 - 18th International Flow Measurement Conference*, pp. 1–5.

differential pressure in wet gas. *Experimental Thermal and Fluid Science*, 79, 245–253. <https://doi.org/10.1016/j.expthermflusc.2016.07.017>

Zheng, X., He, D., Yu, Z., & Bai, B. (2016).

Error analysis of gas and liquid flow rates metering method based on

**Appendix 1: Correlations for WGM using conventional metering devices**

Name	Correlation	Applicability or test condition	Fluids and primary meter
Chisholm (Chisholm, 1977)	$\Phi = \sqrt{1 + C_{Hom}X + X^2}$ $C_{Hom} = \left(\frac{\rho_l}{\rho_g}\right)^n + \left(\frac{\rho_g}{\rho_l}\right)^n, n = 0.25$	$X < 1$	Orifice meter
De Leeuw 1997	$\Phi = 1 + C_{ch}X + X^2$ $C_{ch} = \left(\frac{\rho_g}{\rho_l}\right)^n + \left(\frac{\rho_l}{\rho_g}\right)^n$ $n = 0.41 \text{ for } 0.5 \leq Fr_g \leq 1.5$ $n = 0.606 (1 - e^{-0.746 Fr_g}) \text{ for } Fr_g > 1$	$15 \leq P(\text{bar}) \leq 90$ $\beta = 0.401$ $0.5 \leq Fr_g \leq 4.8$ $0 < X \leq 0.3$ $D = 97.18 \text{ mm}$ $0.014 \leq \rho_g/\rho_l \leq 0.08$	Horizontal Venturi meter NG or Diesel or water or Nitrogen
Smith and Leang 1974	$\Phi = \frac{1}{BF}$ $BF = 0.637 + 0.4211x - \frac{0.00183}{x^2}$ $x = \frac{m_g}{m_g + m_l}$	Steam/water data from Murdock and James	Orifice meter Water/Steam
He and Bai 2014	$\Phi = \frac{K}{1 + X\sqrt{\rho_g/\rho_l}}$ $K = \left[ \frac{0.5681}{\sqrt{\rho_g/\rho_l}} - 0.1444 Fr_g - 0.1494 \right] X +$	$0.01 \leq \rho_g/\rho_l \leq 0.081$ $\beta = 0.6$ $0.6 \leq Fr_g \leq 4.7$ $0 \leq X \leq 0.3$ $D = 2", 8"$	Horizontal Venturi Meter, NG/water NG/Stoddard NG/Stoddard/water NG/kerosene
Steven 2002(R. Steven, 2001)	$A = 2454.51 DR^2 - 389.568 DR + 18.146$ $B = 61.695 DR^2 - 8.349 DR + 0.223$ $C = 1722.917 DR^2 - 272.92 DR + 11.752$ $D = 57.387 DR^2 - 7.679 DR + 0.195$ $DR = \frac{\rho_g}{\rho_l}$ $\Phi = \frac{1 + C_g X + X^2}{1 + C_{nom} X + X^2}$ $C_{nom} = \left(\frac{\rho_g}{\rho_l}\right)^{0.5} + \left(\frac{\rho_l}{\rho_g}\right)^{0.5}$ $C_g = \left(\frac{\rho_g(1-x)}{\rho_l x}\right)^n + \left(\frac{\rho_l x}{\rho_g(1-x)}\right)^n$	$20 \leq P(\text{bar}) \leq 60$ $\beta = 0.55$ $0.4 \leq Fr_g \leq 4$ $0 < X \leq 0.32$ $D = 6"$	Horizontal Venturi Meters, Nitrogen or Eversold80
Lin 1982	$\Phi = 1 + \theta X$ $\theta = 1.48625 - 9.26541 \left(\frac{\rho_g}{\rho_l}\right) + 44.6954 \left(\frac{\rho_g}{\rho_l}\right)^2 - 60.615 \left(\frac{\rho_g}{\rho_l}\right)^3 - 5.12966 \left(\frac{\rho_g}{\rho_l}\right)^4 + 26.5743 \left(\frac{\rho_g}{\rho_l}\right)^5$	$\beta = 0.31, 0.44, 0.62$ $0 < x < 1$ $D = 32 \text{ mm}$ $\frac{\rho_g}{\rho_l} = 0.14, 0.21, 0.24, 0.33$	Orifice meter R-113

<p><b>Lide et al. 2008</b></p>	$n = A + BX^{0.78105}$ $A = 1.29203 \beta^{-0.17161} Fr_g^{0.12618} \left(\frac{\rho_g}{\rho_l}\right)^{-0.011}$ $B = 0.30196 \beta^{0.05205} Fr_g^{-0.07122} \left(\frac{\rho_g}{\rho_l}\right)^{0.021}$ $x = m_g / (m_g + m_l)$ $\Phi = \frac{1 + C_{ch}X + X^2}{C_{wet}}$ $C_{ch} = \left(\frac{\rho_g}{\rho_l}\right)^n + \left(\frac{\rho_l}{\rho_g}\right)^n$	<p><math>1.5 \leq P(\text{bar}) \leq 2.5</math>  <math>0.4048 \leq \beta \leq 0.7</math>  <math>0.67 \leq Fr_g \leq 2</math>  <math>0.0022 \leq X \leq 0.0576</math>  <math>D = 50 \text{ mm}</math></p>	<p>Horizontal Venturi meters, water or air</p>
<p><b>Xu et al. 2012</b></p>	$n = b_1 e^{-0.5 \left[ \left( \frac{\ln(Fr_g/b_2)}{b_3} \right)^2 + \left( \frac{\ln(\frac{\rho_g/\rho_l}{b_4})}{b_5} \right)^2 \right]}$ $b_1 = 0.47359213$ $b_2 = 1.9897702$ $b_3 = 1.8384189$ $b_4 = 0.087328207$ $b_5 = 7.4636959$	<p><math>2.6 \leq P(\text{bar}) \leq 8.6</math>  <math>\beta = 0.45</math>  <math>11.3 \leq U_{sg} \left(\frac{m}{s}\right) \leq 17</math>  <math>0.07 \leq x \leq 0.36</math>  <math>D = 50 \text{ mm}</math></p>	<p>Vertical Venturi meter with extended throat, NG or water</p>
<p><b>ISO/TR 11583:2012</b> (ISO/TR 11583, 2012)</p>	$n = \max(0.583 - 0.18 \beta^2 - 0.578 e^{-0.08 \frac{Fr_g}{H}}, 0.392 - 0.18 \beta^2)$ $C_{wet} = 1 - 0.0463 e^{-0.05 \frac{Fr_g}{\beta^{2.5}}} \min\left(1, \sqrt{\frac{X}{0.016}}\right)$ $H = 1 + 0.35 \left(\frac{\dot{Q}_w}{\dot{Q}_w + \dot{Q}_o}\right); \text{ or } H = 0.79 \text{ steam}$ $\Phi = \frac{1 + C_{ch}X + X^2}{C_{wet}}$ $C_{ch} = \left(\frac{\rho_g}{\rho_l}\right)^n + \left(\frac{\rho_l}{\rho_g}\right)^n$	<p><math>\rho_g/\rho_l \geq 0.02</math>  <math>0.4 \leq \beta \leq 0.75</math>  <math>0 &lt; X \leq 0.3</math>  <math>D \geq 50 \text{ mm}</math>  <math>Fr_g/\beta^{2.5} &gt; 3</math></p>	<p>Horizontal Venturi Meter, Nitrogen/ExxsolD 80          Argon/ExxsolD80          Nitrogen/water          NG/water          NG/Stoddard          NG/Decane          Steam</p>
<p><b>Homogeneous</b> (Collins &amp; Clark, 2013)</p>	$\Phi = \sqrt{1 + C_{Hom}X + X^2}$ $C_{Hom} = \left(\frac{\rho_l}{\rho_g}\right)^n + \left(\frac{\rho_g}{\rho_l}\right)^n, n = 0.5$	<p>N/A</p>	<p>Theoretical mist flow, used for all meter categories</p>
<p><b>Murdock</b> (Murdoch, 1962)</p>	$\Phi = 1 + 1.26X$	<p><math>1 \leq P(\text{bar}) \leq 63</math>  <math>0.26 \leq \beta \leq 0.5</math>  <math>0.041 \leq X \leq 0.25</math>  <math>D = 2.5'' - 4''</math>  <math>1.3 \cdot 10^4 \leq Re_{sg} \leq 1.27 \cdot 10^6</math></p>	<p>Orifice meter, air/water          NG/water          NG/salt water          Steam/water</p>

Sources: Adopted from Chinello (2019)